Systemic Brain Tumor Delivery of Synthetic Protein Nanoparticles for Glioblastoma Therapy

Jason V. Gregory[1,2], Padma Kadiyala[3,4], Robert Doherty[3,4], Melissa Cadena[5], Samer Habeel[5], Erkki Ruoslahti[6,7], Pedro R. Lowenstein[3,4], Maria G. Castro[3,4], and Joerg Lahann[1,2,5]

[1]Biointerfaces Institute, University of Michigan, Ann Arbor, MI, USA. [2]Chemical Engineering, University of Michigan, Ann Arbor, MI, USA. [3]Department of Neurosurgery, University of Michigan Medical School, Ann Arbor, MI, USA. [4]Department of Cell and Developmental Biology, University of Michigan Medical School, Ann Arbor, MI, USA. [5]Biomedical Engineering, University of Michigan, Ann Arbor, MI, USA. [6]Cancer Research Center, Sanford Burnham Prebys Medical Discovery Institute, La Jolla, CA, USA. [7]Center for Nanomedicine and Department of Cell, Molecular and Developmental Biology, University of California, Santa Barbara, Santa Barbara, CA, USA.

Abstract

Glioblastoma multiforme (GBM), the predominant and most aggressive form of brain cancer, has witnessed very little clinical progress over the last decades, in parts, due to the absence of effective drug delivery strategies. Intravenous injection is the simplest and least invasive delivery route to the brain, but has been severely limited by the inability of most GBM drugs to partition through the blood-brain barrier (BBB). Inspired by the capacity of some natural proteins and viral particulates to cross the BBB, we engineered a synthetic protein nanoparticle (SPNP) based on polymerized human serum albumin (HSA) decorated with the cell-penetrating peptide iRGD. SPNPs loaded with siRNA against Signal Transducer and Activation of Transcription 3 factor (STAT3*i*) result in *in vitro* and *in vivo* downregulation of STAT3, a central hub of multiple cancer signaling pathways, which has been associated with GBM progression and inhibition of the immune system, as well as select downstream signals. When combined with the standard of care, i.e., ionized radiation, STAT3*i* SPNPs result in tumor regression and long-term survivors in 87.5% of GBM bearing mice and primes the immune system to develop anti-GBM immunological memory. SPNPs combine the versatility of synthetic nanoparticles with the biological characteristics of protein carriers to establish a major breakthrough in cancer delivery resulting in novel clinical applications in GBM therapy.

Key Words: Protein Nanoparticles, Tumor Targeting, siRNA Delivery, Brain Cancer, Immunomodulatory Materials

Glioblastoma multiforme (GBM) is the most prevalent and aggressive form of brain cancer, currently accounting for approximately 80% of diagnosed brain cancers.[1] GBM is characterized by its high invasiveness, poor clinical prognosis, high mortality rates and frequent recurrence.[2] Current therapeutic approaches include focal radiotherapy, and adjuvant chemotherapeutics in combination with surgical resection. However, due to the delicate anatomical structure of the brain and the highly invasive nature of glioma cells, complete surgical resection is rarely achieved.[3] Residual tumor cells infiltrate the surrounding brain tissue and are protected by the blood-brain barrier (BBB), rendering them unresponsive to conventional chemotherapeutic drugs.[4] Despite recent surgical and chemotherapeutic advances, the median survival (MS) for patients diagnosed with GBM remains just 12-15 months with a 5-year survival rate of 5%. The development of alternative and novel delivery approaches to effectively treat GBM remains one of the most pressing challenges in cancer therapy.[5]

A growing body of evidence suggests that the Signal Transducer and Activator of Transcription 3 (STAT3) pathway is involved in multiple signaling pathways related to tumor progression and evasion of the immune system.[6–8] Multiple growth factors and cytokines frequently overexpressed in cancer, such as EGF, FGF and IL-6, activate STAT3 via tyrosine phosphorylation.[8–10] Activated STAT3 (pSTAT3) translocates to the nucleus and participates in the transcription of genes that inhibit apoptosis, and promote tumor cell proliferation and metastasis. Histopathological analysis of brain tumors demonstrated STAT3 to be overexpressed in patients with grade III astrocytomas and grade IV GBMs; increased STAT3 levels are negatively associated with MS in these patients.[7] In previous studies, the STAT3 inhibitor CPA-7 induced tumor cell death in GL26 mouse GBM and HF2303 human GBM stem cells. However, a positive therapeutic effect was only observed in peripheral tumors, but not in intracranial tumors, pointing towards the inability of CPA-7, like many small molecule

therapeutics and biomolecules, to cross the protective BBB and enter the brain tumor compartment.[6]

A wide range of nanoparticles have been developed to deliver chemotherapeutic drugs, such as docetaxel,[11–13] paclitaxel,[14–16] doxorubicin[17] or other small molecule chemotherapeutics;[18–22] or, to leverage antibodies,[23,24] RNA,[25–28] or peptides[29] in an attempt to enhance GBM therapy. Despite these grand efforts, research conducted over the past decades has made only marginal advances with no real promise of a clinical path towards a viable curative treatment. In general, these nanocarriers share a number of common characteristics, e.g., (i) they are made of synthetic materials, (ii) they tend to accumulate and persist in liver and spleen causing severe side effects, and (iii) they are incapable of passing the BBB. In contrast, natural evolution has resulted in proteins and viral particulates that can target to and transport through the BBB. Inspired by the unique capabilities of biological nanoparticles, we engineered GBM-targeting protein nanoparticles comprised of polymerized human serum albumin (HSA) and oligo(ethylene glycol) (OEG), loaded with the cell-penetrating peptide iRGD[30–32] as well as STAT3*i*. The choice of HSA as the major matrix component was motivated by its rapid and well-understood clearance mechanisms, its demonstrated clinical relevance, and its exquisite biochemical compatibility with both, therapeutic agents and homing peptides. In addition, albumin-based nanocarriers have been shown to engage cell-surface receptors, such as SPARC[33] and gp60,[34] that are overexpressed on glioma cells and tumor vessel endothelium.[35–37]

Particle Design, Synthesis and Characterization

SPNPs were prepared via electrohydrodynamic (EHD) jetting, a process that utilizes atomization of dilute solutions of polymers to produce well-defined nanoparticles.[38–40] Rapid acceleration of a viscoelastic jet in an electric field leads to a size reduction by several orders of

magnitude facilitating rapid solvent evaporation and solidification of the non-volatile components into nanoparticles. Here, the jetting solution was comprised of human serum albumin and a bifunctional OEG macromer (NHS-OEG-NHS, 2kDa), which were mixed with various additional components, such as a therapeutic siRNA, polyethyleneimine (PEI, a siRNA complexing agent), and the tumor penetrating peptide, iRGD, prior to nanoparticle preparation. The OEG macromer underwent step-growth polymerization with albumin molecules through reaction with its lysine residues resulting in water-stable nanoparticles. After EHD jetting and collection, the resulting SPNPs had an average diameter of 115 ± 23 nm in their dry state (Fig. 1b). Once fully hydrated, the average diameter of SPNPs increased to 220 ± 26 nm based on dynamic light scattering (DLS) measurements (Supplementary Fig. 1). The degree of nanoparticle swelling was controlled by varying the HSA-to-OEG ratios between 4:1 and 20:1 and the molecular weight of the OEG macromer between 1 kDa and 20 kDa. An increase of the OEG content from 5% to 20% resulted in a reduction of particle swelling by 20 volume-%. SPNPs were stable for at least 10 days at 37 °C under physiological conditions; with no significant change in particle size or morphology (Supplementary Fig. 2). When exposed to mildly acidic conditions (pH 5.0), similar to those observed in endosomes of cancer cells, the diameters of SPNPs increased to 295 ± 31 nm (Fig. 1c). We note that defining particle properties, such as particle size, shape and swelling behavior, was, within the margins of error, identical for fully loaded SPNPs, empty nanoparticles and nanoparticles loaded with siRNA and/or iRGD.

In Vitro Cell Uptake and siRNA Activity

Previously, co-delivery of the cell-penetrating peptide iRGD has increased tumor targeting for both, small drugs and iron oxide nanoparticles.[41] The iRGD peptide has been shown to act in a three-stage process, first binding to $\alpha v\beta 3$ and $\alpha v\beta 5$ integrins, followed by a proteolytic cleavage

step and a secondary binding event to neurophilin-1 (NRP-1), which activates an endocytotic/exocytotic transport pathway.[42] In the past, iRGD mediated tumor homing has been approached either in form of systemic co-delivery of iRGD with nanoparticles[43,44] or by decorating the nanoparticles with surface-bound iRGD.[45,46] In our case, the iRGD peptide is preloaded into SPNPs during EHD jetting to promote local release at the vicinity of the BBB. To investigate the intracellular fate of nanoparticles and the effect of iRGD as a targeting ligand, in vitro uptake experiments were performed. When iRGD-loaded SPNPs were incubated with GL26 glioma cells for a period of 30 minutes, particle uptake increased by ~ 5-fold compared to nanoparticles without iRGD (Fig. 1e). Image analysis of 3D confocal images (Fig. 1d) using CellProfiler revealed that significantly less particles colocalized with lysosomes of GL26 glioma cells compared to nanoparticles without iRGD (Fig. 1f). These data suggest that the delivery of iRGD from SPNPs results in higher uptake and higher cytosolic nanoparticle concentrations. The above-mentioned pH-dependent swelling of SPNPs, along with the “proton sponge” effect previously postulated for PEI,[47] may contribute to more effective particle escape from endocytotic vesicles, enhancing overall siRNA delivery to the cytosol and RNA-induced silencing.[48,49]

We next evaluated if siRNA loaded into SPNPs during EHD jetting remains biologically active. First, siRNA loading and release from SPNPs was evaluated using a Cy3-labeled STAT3*i* surrogate. Utilizing stimulated emission depletion (STED) microscopy, we confirmed uniform distribution of siRNA throughout the entire NP volume (Supplementary Fig 3). *In vitro* release of fluorescently tagged siRNA confirmed that 96% of the initial amount of siRNA was encapsulated into SPNPs; corresponding to a siRNA loading of 340 ng, or 25 pmol of siRNA per mg of SPNPs. Furthermore, we observed that approximately 60% of the encapsulated siRNA was released over the first 96 hours, followed by a sustained release period progressing for 21 days

(Supplementary Fig. 4). When albumin NPs were loaded with siRNA against GFP, SPNPs significantly suppressed GFP expression in mouse glioma cells transfected to express mCitrine (GL26-Cit, Supplementary Fig. 5) relative to control albumin NPs loaded with scrambled siRNA or free GFP siRNA that was delivered using lipofectamine as the transfection agent. Moreover, protein knockdown persisted significantly longer in the SPNP group than in lipofectamine-transfected cells (Supplementary Fig. 5). While the latter entered a recovery phase after two days and nearly returned to normal GFP levels by day five, cells treated with GPF*i* SPNPs showed sustained protein knockdown throughout the experiment. There were no significant differences in particle size, surface charge, or morphology between siRNA-loaded SPNPs and the control particles.

For particle concentrations of 2.5 and 25 ug/mL, SPNPs co-loaded with iRGD and STAT3*i* significantly reduced total STAT3 protein expression relative to the untreated control group or empty SPNPs (Fig. 1g). Moreover, we observed a dose-dependent response in that a higher particle concentration resulted in ~ 2-fold further decrease in total STAT3 expression. No detectable signs of cytotoxicity were observed for any of the tested NP groups, which we attributed to the fact that the delivered siRNA concentrations were below the cytotoxicity limit observed for free STAT3 siRNA in GL26 cells (Supplementary Fig. 6). Based on these *in vitro* experiments, we chose an effective dose of 5 μg/kg in subsequent animal studies.

Systemic Delivery of SPNPs in an Intracranial GBM Model

In the past, the BBB has been an unsurmountable delivery challenge for nanocarriers[50,51] that are systemically administrated via IV injection. To evaluate, if systemically delivered SPNPs can home to brain tumors, SPNPs loaded with Alexa Fluor™ 647-labeled albumin were prepared as

described above. In the absence of large animal GBM models, we selected the very aggressive GL26 syngeneic mouse glioma model, which is known to exhibit histopathological characteristics encountered in human GBM,[52] to evaluate GBM-targeting of SPNPs. In addition, this model features an uncompromised immune system, which was deemed to be essential, because of the prominent role that STAT3 plays in downregulation of the immune system. A dose of 2.0 x 10^{13} SPNPs was delivered to GBM-bearing mice via a single tail vein injection seven days after glioma cell (GL26-Citrine) implantation in the right striatum of the mice (Fig. 2a). After 4 or 24 hrs, animals were euthanized, and brains were collected, sectioned, and stained prior to confocal imaging. While the majority of particles was taken up by other organs, such as liver, kidney, spleen and the lungs, a significant number of SPNPs appeared to have crossed the BBB and were identified within the brain tumor microenvironment at both time points (Fig. 2b). Tumor targeting was markedly increased after 24 hrs, hinting towards the possibility that secondary transport processes, such as transcytotic or immune-cell-mediated BBB pathways, are contributing to the brain-homing of SPNPs, in addition to the direct targeting of the brain endothelium by circulating nanoparticles. The notion of a multivariant transport mechanism is consistent with our finding that SPNPs were localized inside of tumor cells (green) and macrophages (red), suggesting that both cell types can internalize SPNPs (Fig. 2b).

Using the same intracranial tumor model, GBM specific biodistribution of SPNPs was assessed. Tumor-bearing mice were injected three times (7d, 10d, and 13d DPI) with Alexa Fluor 647-labeled SPNPs or nanoparticles without iRGD (Fig. 2c). In addition, naïve mice (non-tumor bearing) were subjected to the same regimen to delineate tumor-specific characteristics. After 14 days, naïve and tumor bearing mice were euthanized, their main organs were collected, and the nanoparticle distribution was analyzed via fluorescence imaging (Fig. 2d). In both GBM-bearing and naïve mice, significantly more SPNPs were observed in the brain compared to

nanoparticles without iRGD. As expected, SPNPs also accumulated in the lungs and liver – independent of the particular experimental group. The former can be attributed to being the first capillary bed the NPs would encounter following intravenous injection, while the latter represents the primary route of clearance for NPs of this size.[53] Brain accumulation of SPNPs loaded with iRGD was higher for both naïve and GBM-bearing mice compared to iRGD-free nanoparticle groups. When directly comparing SPNPs localization within the brain compartment, the accumulation of iRGD-loaded SPNPs was 40% higher in tumor-bearing brains (Fig. 2e) than in healthy brains.

To provide a rationale for the increased accumulation of SPNPs in the brains of tumor-bearing mice, we searched for integrin-expressing cells in the tumor microenvironment. Specifically, we focused on the relative expression of $\alpha v\beta 3$ and $\alpha v\beta 5$ integrins, because these ligands have been shown to play pivotal roles in the iRGD-induced accumulation of nanoparticles and small drugs in tumors,[30] and are overexpressed in gliomas.[31] Using the GBM model and dosing schedule from the biodistribution studies, brains from GBM tumor-bearing mice were collected at 23 DPI. Normal brain and tumor tissue were dissected from the brain, processed, and stained with $\alpha v\beta 3$ and $\alpha v\beta 5$ antibodies for flow cytometry analysis. More than 60% of the GBM tumor population expressed $\alpha v\beta 3$ and $\alpha v\beta 5$ integrins at high levels, while normal brain cells showed minimal expression of these proteins. These results, along with the observed differences in brain accumulation in the biodistribution study, appear to be consistent with the previously postulated hypothesis that iRGD promotes local brain tumor accumulation.[42]

In vivo Survival Studies

To test the efficacy of SPNPs *in vivo*, GBM-bearing mice were treated intravenously with multiple doses of STAT3*i* SPNPs over the course of a three-week treatment regimen (Supplemental Fig. 9). After tumor implantation, the median survival (MS) of untreated mice was about 28 days. In mice that received multiple doses of empty SPNPs, the MS remained unaltered (28 days). In contrast, when SPNPs loaded with STAT3*i* were administered, the MS increased to 41 days, a statistically significant increase of 45%. Delivery of the same doses of free STAT3*i* resulted in a modest extension of MS by 5 days, which is likely too low to elicit a significant therapeutic effect. The low efficacy of free STAT3*i* can be explained by the rapid degradation of genetic material following systemic administration – in addition to siRNA's inability to cross the BBB.[54]

Encouraged by the prospect of a nanoparticle formulation for STAT3*i* delivery with significant *in vivo* efficacy, we combined STAT3*i* SPNPs with the current standard of care, i.e., focused radiotherapy (IR). Previous studies have identified a direct correlation between STAT3 overexpression and radioresistance in other cancers,[55,56] suggesting that its knockdown could contribute to enhanced efficacy. We thus established a treatment protocol that combined the previously evaluated multi-dose regimen with a repetitive, two-week focused radiotherapy regimen (Fig. 3a). Once GBM tumors had formed, mice received seven doses of STAT3*i* SPNPs over the course of a three-week period. During each of the first two weeks, mice also received five daily 2 Gy doses of IR for a total of ten treatments (Fig. 3a). Experimental groups included mice that received either STAT3*i* SPNPs, empty SPNPs, free STAT3*i*, or saline with or without combined radiotherapy. In all cases, the addition of radiotherapy increased the MS, with IR alone resulting in a MS extension from 28 to 44 DPI (Fig. 3b). Combining IR with empty SPNPs did not further alter the MS. Consistent with our previous experiment, free siRNA provided a slight, statistically significant benefit, where the MS was increased to 58 DPI, when

combined with IR (Fig. 3b, brown line). However, a much more dramatic effect was observed for the combination of STAT3*i* SPNPs with IR. Of the eight mice in this group, seven reached the standard long-term survivor time point of 90 DPI and appeared to be completely tumor-free thereafter (Fig. 3b, blue line). The single mouse receiving this treatment that did not reach long-term survival was moribund at 67 DPI, longer than any other non-surviving subject from all other groups.

In order to fully characterize the effects of the combined treatments, several analyses were performed. Initially, we elucidated the expression of STAT3 and its active phosphorylated form, pSTAT3, in the brain tissues (Fig. 3c). As expected, the greatest reduction in both the total and phosphorylated form of the protein were found in the STAT3*i* SPNP group. Greater than 50% reduction in total STAT3 protein was present, compared to the saline treated control. Phosphorylated STAT3 levels were even more dramatically reduced, with a greater than ten-fold reduction in pSTAT3 levels comparing the same groups. In contrast, the total STAT3 levels were relatively unchanged in both, the free STAT3*i* and empty SPNP groups, compared to untreated control. Here, pSTAT3 was increased by 110% for empty SPNPs, suggesting a shift in the balance of the two forms, perhaps due to a localized upregulation of kinase activity.

Immunohistochemistry (IHC) analysis was used to compare the brains from long-term survivors to other treatment groups. Fig. 3d shows a direct comparison of the brain of a long-term survivor and that of a control animal that did not receive treatment. Hematoxylin and eosin (H&E) staining clearly shows the presence of a fully developed tumor localized within a single hemisphere of the saline treated mice. Conversely, we observe no overt signs of tumor presence in the STAT3*i* SPNP + IR treated survivors (Fig. 3d, top). Moreover, no apparent regions of necrosis, palisades or hemorrhages were present in these animals 90 DPI after

receiving a full course of therapy. Myelin basic protein (MBP) staining was performed to assess the possible disruption of the surrounding brain architecture due to the treatment. No apparent changes in oligodendrocyte integrity was observed in mice that received the combined STAT3*i* SPNP + IR treatment when compared to the cancer-free right faces of mice in the saline treated control group (Fig. 3d, middle). In addition, CD8 T cells were sparse in the TME (Fig. 3d, bottom) and their total number was significantly reduced in STAT3*i* SPNP + IR treated mice compared to the saline treated control group (Supplementary Fig. 10). Independent pathological analysis of potential side effects affecting the livers of mice treated with STAT3*i* SPNP + IR therapy found minimal to mild monoculear pericholangitis across all groups and characterized it as spontaneous background rather than a direct result of the applied therapy. (Supplementary Fig. 11). In all treatment groups, with the exception of the saline treated control, minimal to mild coagulative necrosis was present. In the treatment group that received free STAT3*i*, one animal displayed multiple foci of coagulative necrosis, which distinguished it from all other animal in the entire study cohort, including those from the combined STAT3*i* SPNP + IR group, where the regions of necrosis were generally small and were deemed not to induce a biologically significant effect on liver function.

Next, SPNP-induced immune responses were assessed using a modified enzyme-linked immunosorbent assay (ELISA, Supplementary Fig. 12). To avoid a species-to-species mismatch due to the use of human serum albumin in mice, otherwise identical NPs were synthesized, in which HSA was replaced with mouse serum albumin (MSA). No circulating antibodies specific to MSA SPNPs were observed in any of the treatment groups (Supplementary Fig. 12) indicating neglectable immunogenicity against any of the individual components of SPNPs, such as OEG, STAT3*i*, iRGD, or PEI. As expected, replacing MSA with HSA resulted in elevated levels of HSA antibodies for both, STAT3*i* SPNP and empty SPNP treatment groups (Supplementary Fig. 12).

However, free STAT3*i* therapy did not induce this same response suggesting that antibodies were formed in response to the exposure of the nanoparticles rather than the active therapeutic ingredient.

To further investigate the potential role of the adaptive immune system, we more closely examined the population of CD8 T cells within the tumor microenvironment (TME) via flow cytometry. We established tumors in mice using GBM cells that harbored a surrogate tumor antigen ovalbumin and compared the responses elicited by the various treatment formulations (Fig 3e). Tumor specific T cells in the TME were characterized by staining for the SIINFEKL-H2K^b-OVA tetramer, an OVA cognate antigen within the CD8 T cell population. Tumor specific CD8 T cells (CD3 + / CD8 + /SIINFEKL-H2K b tetramer) within the STAT3*i* SPNP + IR group were increased by twofold compared to all other groups (Fig. 3f, top). Staining the same population of cells with INF-γ and granzyme B (GZB) revealed an twofold increase in cytotoxic T cells in the TME (Fig. 3f, middle and bottom) in the STAT3*i* SPNP + IR group relative to all other groups. Taken together, these results suggest a robust anti-GBM response elicited by the combined NP + IR therapy that is likely contributing to the observed therapeutic success.

Flow cytometry analysis of tumor infiltrating macrophages and conventional dendritic cells (cDCs:CD45 + /CD11c + / B220 -) was used to compare treatment groups containing free STAT3*i*, empty SPNP and STAT3*i* SPNPs in combination with IR (Fig. 4a and 4b). Co-staining of CD45$^+$ cells with F4/80 and CD206 antibodies was used to establish a subpopulation of tumor associated macrophages (TAMs). Within the TAM population, both, M1 (CD45 + /F4/80 + / CD206 -) and M2 (CD45 + /F4/80 + / CD206 +) macrophage phenotypes, were identified for all cohorts, but their relative abundance was significantly different in the STAT3*i* SPNP + IR group

compared to all other groups. In the STAT3*i* SPNP + IR group, M1 macrophages were increased by 2.5-fold (Fig. 4c, left), whereas the number of M2 macrophages was decreased by three- to four-fold decrease (Fig. 4c, middle). These findings are consistent with the notion that the STAT3*i* SPNP + IR treatment selectively decreases the tumor suppressive M2 macrophage subpopulation. In addition, antigen presentation by cDCs was significantly higher in animals receiving STAT3*i* SPNPs compared to free siRNA and empty SPNPs (Fig. 4c, right). IR treatment further elevated this effect resulting in the largest cDC population for the STAT3*i* SPNP + IR group. Co-staining of CD45 and F4/80^{high} cells with CD206 and Arg1 antibodies in the STAT3*i* SPNP + IR group confirmed that the vast majority of TAMs were of the M2 phenotype (Supplemental Fig. 13). Among all TME CD45^{+} immune cells, only M2 macrophages displayed the far-red Alexa Fluor 647 signal indicative of SPNPs suggesting that M2 macrophages are the primary TME-based immune cells that internalize SPNPs (Supplemental Fig. 14).

Tumor Re-challenge Study

Current standard of care approaches, including surgical resection combined with focused radiation and the chemotherapeutic temozolomide, have been used to treat primary GBM tumors. However, owning to the aggressive and infiltrative nature of GBM, these patients, as a rule, experience recurrence contributing to the high mortality and dismal survival rates. Based on the encouraging immune response observed in our survival study, we chose to re-challenge survivors from the STAT3*i* SPNP + IR treatment group. Tumors were implanted in the contralateral hemisphere of mice that were previously cured by the STAT3*i* SPNP + IR therapy. These mice did not receive any additional intervening therapy (Fig. 4d). As a control, naïve mice were also implanted with tumors at the same timepoint and likewise received no treatment. As expected, the control group saw rapid tumor growth, increased signs of disease and had a

median survival of 27 DPI. Despite not receiving any additional treatment, all re-challenged mice survived to a second long-term survival point of 90 DPI (relative to the second tumor implantation, 180 days post initial tumor implantation) (Fig. 4e). IHC analysis of the brains yielded comparable results (Fig. 3f). H&E staining clearly showed the formation of a fully developed tumor mass in the control group, while members of the re-challenged cohort displayed no regions of necrosis, palisades or hemorrhages in either hemisphere (Fig. 4f, top). MBP staining confirmed that there was no overt disruption of the surrounding brain architecture (Fig. 4f, middle). Lastly, the presence of CD8 T cells was observed to be five-fold lower (Supplemental Fig. 15) in the STAT3*i* SPNP re-challenge group compared to the control (Fig. 4f, bottom). Importantly, we found no adverse effects in the brains of re-challenged survivors. Our findings suggest the potential involvement of an adaptive immune response that appears to guard against secondary tumors; an essential condition of any successful GBM therapy which will require long-term eradication of migrating and resistant CSCs, typically missed by traditional therapies.

Conclusions

The main clinical challenge of GBM therapy is the lack of effective delivery systems that provide long-lasting health benefits for patients. A wide range of experimental approaches have been proposed in recent years based on either systemic or intracranial delivery strategies. To date, experimental studies that report even modest levels of efficacy are scarce and almost exclusively require invasive convection-enhanced intracranial delivery.[18,25] As for systemic delivery, the situation is even more troublesome with only a couple of studies reporting long-term survivors at all.[12,29] SPNPs combine the biological benefits of proteins with the precise engineering control of synthetic nanoparticles to yield (i) high efficacy (87.5% long-term survivors in a very aggressive intracranial tumor model), (ii) effective tumor delivery using

systemically administered nanoparticles, and (iii) novel possibilities towards long-term eradication of resistant cancer cells using immunomodulatory protein nanoparticles. While protein-based nanoparticles have been a fairly uncharted area of research, this study demonstrates that synthetic nanoparticles that use proteins as structural building blocks may pave a novel route towards clinical cancer therapy. We studied the nanoparticle-mediated delivery of a siRNA against STAT3 (STAT3*i*), but the SPNP platform could be adopted, with further work, for delivery of small-molecule drugs, other siRNA therapies, or even drug combinations to a wide variety of solid tumors.

Table 1: Recent advances in NP-based GBM therapy.

Author (Year)	Vehicle	Therapeutic	Targeting Moiety	Delivery Method	Model Animal	Cell Type (Species)	MS vs. Control, (% over control)	Long-term Survivors (%)	Ref.
Gajbhiye et al. (2011)	PPI dendrimers	Docetaxel	Polysorbate 80	Systemic IV	Albino Rats	Stereotactically Implanted U87MG (H)	42 vs. 14 (300%)	0.0%	[6]
Gao et al. (2012)	PEG-PCL NPs	Docetaxel	GMT8	Systemic IV	Nude mice	Stereotactically Implanted U87 (H)	40 vs. 22 (182%)	33% (2/6)	[7]
Shi et al. (2015)	PLGA NPs	Docetaxel	RGD peptide	Systemic IV	SD Rats	Stereotactically Implanted C6 (R)	57 vs. 16 (356%)	0.0%	[8]
Ganipineni et al. (2019)	Magnetic Polymer NPs	Paclitaxel	RGD peptide	Systemic IV	NMRI nude mice	Stereotactically Implanted U87MG (H)	46 vs. 38 (121%)	0.0%	[9]
Kang et al. (2015)	PLGA-PEG NPs	Paclitaxel	CRT peptide	Systemic IV	Nude mice	Stereotactically Implanted C6 (R)	46 vs. 21.5 (214%)	0.0%	[10]
Kang et al. (2016)	Polymeric NPs	Paclitaxel	FHK/tLyp-1 peptide	Systemic IV	BALB/c nude mice	Stereotactically Implanted U87 (H)	59 vs. 16 (368%)	0.0%	[11]
Yang et al. (2012)	Liposomes	Doxorubicin	AP-1 peptide	IV + HIFU	NOD-*scid* mice	Stereotactically Implanted GBM8401 (H)	15 vs. 9 (166%)	0.0%	[12]
Zhou et al. (2013)	PLGA NPs	Dithiazanine iodide	-	Convection enhanced delivery	Immunocompromised rats	Stereotactically Implanted U87MG (H)	280 vs. 147 (190%)	66.6% (4/6)	[13]
Householder et al. (2015)	PLGA NPs	Camptothecin	-	Systemic IV	C57CL/6 albino mice	Stereotactically Implanted GL261 (M)	36.5 vs. 28 (130%)	0.0%	[14]
Gaudin et al. (2016)	Squalenoyl NPs	Gemcitabine	-	Convection enhanced delivery	Male Fischer 344 Rats	Stereotactically Implanted RG2 (R)	22 vs. 13 (169%)	0.0%	[15]
King et al. (2017)	PLA-PEG NPs	VE822	-	Convection enhanced delivery	Male Fischer 344 Rats	Stereotactically Implanted RG2 (R)	23 vs. 14 (164%)	0.0%	[16]
Zhang et al. (2015)	Liposomes	Epirubicin	cRGD	Systemic IV	BALB/c nude mice	Stereotactically Implanted U251 (H)	28 vs. 17.5 (160%)	0.0%	[17]
Kaluzova et al. (2015)	Iron-oxide NPs	-	Cetuximab	Convection enhanced delivery	Athymic nude mice	Stereotactically Implanted LN229wtEGFR (H)	73 vs. 29 (251%)	0.0%	[18]
Bouras et al. (2015)	Iron-oxide NPs	-	Cetuximab	Convection enhanced delivery	Athymic nude mice	Stereotactically Implanted U87MGEGFRvIII (H)	60 vs. 15 (400%)	0.0%	[19]
Cohen et al. (2015)	Lipid NPs	PLK-1 siRNA	Hyaluronan	Intratumoral	Athymic BALB/c nu/nu mice	Stereotactically Implanted U87MG (H)	Undefined v 33 (-)	60%	[20]
Danhier et al. (2015)	Chitosan-Lipid NPs	Galectin1/EGFR siRNAs	-	Convection enhanced delivery	Female athymic Swiss nude mice	Stereotactically Implanted U87MG (H)	39 vs. 32 (121%)	0.0%	[21]
Erel-Akbaba et al. (2019)	Solid Lipid NPs	PD-L1 / EGFR siRNAs	iRGD	Retro orbital	C57CL/6 mice	Stereotactically Implanted GL261-Fluc (M)	38 vs. 21 (181%)	0.0%	[22]
Seo et al. (2019)	PLA-HPG NPs	miR-21	ApoE	Convection enhanced delivery	Male RNU Rats	Stereotactically Implanted U87 (H)	50 vs. 24 (208%)	25% (4/16)	[23]
Agemy et al. (2001)	Iron-oxide NPs	KLAKLK peptide	CGKRK + iRGD (CoAdmin.)	Systemic IV	NOD-SCID Mice	H-RasV12-shp53 Lentiviral Induced GBM (-)	Undefined vs. 60 (-)	90% (9/10)	[24]
						Stereotactically Implanted U87 (H)	85 vs. 32 (265%)	0.0%	

Materials and Methods

Table 2. Particle Synthesis Materials

Material	Source	Catalog Number
Human Serum Albumin	Sigma Aldrich	A3782
O,O′-Bis[2-(N-Succinimidyl-succinylamino)ethyl]polyethylene glycol	Sigma Aldrich	713783
Ethylene Glycol	Sigma Aldrich	324558
UltraPure DNase/RNase-Free Distilled Water	Thermo Fisher	10977015
Albumin from Bovine Serum Alexa Fluor 647 Conjugate	Thermo Fisher	A24785
Albumin from Bovine Serum Alexa Fluor 488 Conjugate	Thermo Fisher	A13100
Silencer GFP (eGFP) siRNA	Thermo Fisher	AM4626
Silence Cy3-labeled Negative Control siRNA	Thermo Fisher	AM4621
SignalSilence STAT3 siRNA I Mouse	Cell Signaling	6353
Polyethyleneimine	Sigma Aldrich	181978
iRGD peptide	Ruoslahti Lab	N/A

Table 3. Capillary Immunoassay Reagents / Antibodies

Material (Antibody / Dilution)	Source	Catalog Number
Beta Actin (13E5) Rabbit mAb 1:50	Cell Signaling	4970
STAT3 (D3Z2G) Rabbit mAb 1:50	Cell Signaling	12640
Phospho-STAT3 (Tyr705) (D3A7) XP Rabbit mAb 1:50	Cell Signaling	9145
BcL-xL (54H6) Rabbit mAb 1:50	Cell Signaling	2764
Cyclin-D1 (92G2) Rabbit mAb 1:50	Cell Signaling	2978
Survivin (71G4B7) Rabbit mAb 1:50	Cell Signaling	2808
BcL-2 (D17C4) Rabbit mAb 1:50	Cell Signaling	2876
McL-1 (D2W9E) Rabbit mAb 1:50	Cell Signaling	9429

Table 4. Immunofluorescence Reagents

Material	Source	Catalog Number
Anti-LAMP1 Antibody [EPR21026] 1:100	abcam	ab208943
Goat Anti Rabbit IgG HL Alexa Fluor 555 1:200	abcam	ab150078
Prolong Diamond Antifade Mountant with DAPI	Thermo Fisher	P36966

Table 5. Flowcytometry Antibodies

Antibodies / Dilution	Source	Catalog Number
V450 rat anti mouse CD45, Flow 1:200	BD Bioscience	560501
PE Rat anti mouse F4/80, Flow 1:200	Biolegend	123110
Alexa Fluor 700 Rat anti mouse CD206, Flow 1:200	Biolegend	9661
PE armenian hamster anti mouse CD11C, Flow 1:200	Biolegend	117308
PercpCy5.5 rat anti mouse B220, Flow 1:200	Biolegend	103236
FITC rat anti mouse CD8, Flow 1:200	Biolegend	100706
PercpCy5.5 armenian hamster anti mouse CD3, Flow 1:200	Biolegend	100328
PB rat anti mouse Granzyme B, Flow 1:200	Biolegend	515407
PE rat anti mouse IFNγ, Flow 1:200	Biolegend	505808
PE-Tetramer, Flow \1:100	MBL International	TB-5001-1
Efluor 780-Live/Dead, Flow 1:200	Affymetrics	65-0865-14

Table 6. Immunohistochemistry Primary Antibodies

Antibodies / Dilution	Source	Catalog Number
Rat anti mouse MBP, IHC 1:300	Millipore	MAB386
Rabbit anti mouse CD8, IHC: 1: 2000	Cedarlane	361003
Rat anti mouse F4/80, IHC: 1:500	BioRad	MCA497RT

Table 7. Immunohistochemistry Secondary Antibodies

Antibodies / Dilution	Source	Catalog Number

Goat polyclonal anti-rabbit biotin-conjugated, IHC 1:1000	Dako	E0432
Goat polyclonal anti-rat Alexa Fluor 594, IHC 1:1000	Thermo Fisher	A-11007
Goat polyclonal anti-rabbit biotin-conjugated, IHC 1:1000	Thermo Fisher	31830

Table 8. Reagents for Cell Culture

Reagent	Source	Catalog Number
Dulbecco's Modified Eagle Medium (DMEM)	Thermo Fisher	12430054
heat-inactivated fetal bovine serum (FBS)	Atlanta Biologicals	S11150
Penstrep (10,000U/mL)	Thermo Fisher	15140122
G418	Thermo Fisher	10131035
Trypsin-EDTA (0.05%), phenol red	Thermo Fisher	25300054
DPBS, no calcium and no magnesium	Thermo Fisher	14190144

Synthesis of STAT3 siRNA-loaded, IRGD-functionalized albumin nanoparticles.

Albumin nanoparticles were fabricated via the electrohydrodynamic (EHD) jetting process previously established in our group. Briefly, for all particle types, human serum albumin (HSA) was dissolved in a cosolvent mixture (80:20 v/v) of ultrapure water and ethylene glycol at a concentration of 7.5 w/v%. A bifunctional OEG (NHS-OEG-NHS, 2kDa) was added at 10 w/w% relative to HSA. When iRGD was incorporated in the nanoparticles, 355 ng per mg of albumin was added directly to the jetting solution. In contrast, when incorporating siRNA into the particles, the siRNA was first complexed with a branched polyethyleneimine (bPEI, 60 kDa) for 30 minutes in ultrapure water and the mixture was then added to the jetting solution resulting in 0.04 mg and 355 ng (26 pmol) of bPEI and siRNA per mg of protein nanoparticle, respectively. In instances when siRNA was not included (control nanoparticles) an addition of bPEI in ultrapure water was still included. Final jetting solutions were pumped through a syringe equipped with a 26-gauge blunt tip needle at a flowrate of 0.1 mL/h while a constant voltage (ranging from 7.5 to 9.0 kV) was applied to form a stable Taylor cone at the needle tip. Particles were collected in aluminum pans at a needle to collector distance of 15 cm and then incubated for seven days at 37ºC to facilitate complete polymerization. Albumin NPs were then stored in dark RT conditions in their dry state for future experiments.

Collection and purification of albumin nanoparticles

Albumin NPs were collected according to a standard protocol developed in our lab. In brief, a small volume, 5-10 mL, of water:ethanol (80:20 v/v) + 0.5% Tween 20, was added to the aluminum pans containing EHD jetted NPs. The resulting NP suspension was gently sonicated to disperse any aggregates and passed through a 40 μm cell straining filter. The resulting solution was centrifuged at 4,000 rpm (3,220 rcf) for 4 minutes to pellet and remove any albumin aggregates larger than 1 μm in diameter. The supernatant was then divided into 2 mL

Eppendorf tubes and centrifuged at 15,000 rpm (21,500 rcf) to concentrate the samples to a single 1 mL sample for use in planned experiments. Collected NPs were used within 1 week of their collection and were stored at 4°C during that time.

Characterization of albumin NPs size, shape, and concentration

Albumin nanoparticles were characterized prior to their use in any experiments to ensure they met specifications. Physical characterization included the measurement of particle size in both their dry and hydrated state. To measure particle diameter and investigate their morphology, small silicon wafers were placed on the grounded collection surface and were subjected to the same incubation period to complete the step-growth polymerization. These samples were imaged via Scanning Electron Microscopy (SEM) using a FEI NOVA 200 SEM/FIB instrument. NPs in their hydrated state were collected and purified as described above. The stock solution was diluted in PBS + 0.5% Tween 20 for subsequent measurements using DLS (dynamic light scattering) and NTA (nanoparticle tracking analyzer) to investigate size and solution concentration. Albumin NP solution concentration was further validated using the BCA (bicinchoninic acid) assay.

Albumin NP stability and swelling characterization

Albumin NPs collected and purified as described above were studied to determine their swelling behavior in response to changes in pH and stability in their hydrated state. NPs from the concentrated stock solution were diluted into either a solution of PBS + 0.5% Tween 20 (pH 7.4) or sodium acetate – acetic acid buffer +0.5% Tween 20 (pH5.0). The final NP solutions were stored at 37°C for a period of 10 days. Particle diameter was measured throughout this period to compare the particle size distribution in response to acidic vs. neutral pH conditions and their overall stability at physiological temperatures.

Loading and release of siRNA from albumin nanoparticles

To validate siRNA loading and characterize its release from the albumin NPs, a fluorescently labeled, Silencer Cy™3-labeled negative control siRNA was incorporated into the NP formulation following the same process as described above. NPs were incubated and collected as previously described. To validate siRNA incorporation into the particles, a Alexa Fluor™ 488 BSA conjugate was added at 0.5% of the total albumin mass. Colocalization of the fluorescent albumin NP and siRNA were confirmed using super-resolution STED (stimulated emission depletion) microscopy. Release of the same fluorescent siRNA was conducted over a period of 4 days in PBS +0.5% Tween at 37°C. The supernatant was analyzed using a Horiba fluorimeter and compared against a previously generated calibration curve.

Cell line and cell culture conditions

GL26, GL26-Cit, and GL26-OVA glioblastoma cells were cultured in Dulbecco's modified eagle (DMEM) media supplemented with 10% fetal bovine serum (FBS), 100 units/mL penicillin, and 0.3 mg/mL L-glutamine. For mCitrine and OVA selection, culturing medium was additionally supplemented with 6μg/mL G418. Cells were passaged every 2-3 days and were maintained in a humidified incubator at 95% air/5% CO2 at 37°C.

Immunofluorescence uptake/lysosome colocalization

To study the effect iRGD has on particle fate upon uptake by glioma cells, GL26 cells were cultured as previously described in 4-well Nunc™ Lab-Tek™ Chamber Slides. Cells were seeded at 50,000 cells per well and allowed to adhere overnight. Twelve hours after initial seeding, media was exchanged. Fresh media contained either iRGD albumin NPs or albumin NPs (without iRGD), each labeled by incorporating an Alexa Fluor™ 647 BSA, at a concentration of 13.3 μg NPs per mL. Thirty minutes after particle administration, the media was removed, cells were washed three times with warm PBS, and fresh NP-free media was then added to each well. Cells were cultured normally for an additional three hours before the cells were washed,

fixed and stained. In brief, cells were washed with PBS and fixed in 2% paraformaldehyde in PBS for 15 minutes and then permealized with 0.1% Triton X-100 in PBS for an additional 15 minutes. Cells were then rinsed three times with PBS, and five times with PBS + 0.5% BSA (PBB) and blocked with a one hour incubation in 2% BSA in PBS. Following a rinse with fresh PBB, cells were incubated with primary antibody for LAMP-1, a lysosomal marker, at 5 μg/mL in a PBB solution at room temperature for one hour. After five rinses with fresh PBB, a mixture of Goat Anti-Rabbit IgG H&L Alexa Fluor™ 555 and Phalloidin Alexa Fluor™ 488, prepared in PBB was added and incubated for one hour at room temperature. Each well was rinsed five times with PBB, incubated for one minute with Hoescht at 0.01 mg/mL in DI water, and washed three times with fresh PBS. Finally, the chamber potion of the device was removed, the glass slide allowed to dry and samples were mounted using Prolong™ Diamond Antifade Mountant to preserve the samples and protect against fluorescent signal bleaching.

Once stained and mounted each sample was imaged using CLSM (confocal laser scanning microscopy). Settings for all samples were optimized and kept consistent from sample to sample. Z-stack images were collected from multiple regions within each well and the resulting three dimensional images were analyzed using an established protocol and the CellProfiler software. Analyzed data was used to calculate the relative number of NPs internalized by the cells and the percent of these cells colocalized within the lysosomes.

In vitro GFP silencing via albumin nanoparticle delivered siRNA

As a preliminary experiment, to validate the ability of siRNA delivered via the albumin NPs, particles loaded with siRNA against GFP were synthesized as described above. GL26-cit cells were cultured according to a previously described protocol. Twelve hours after initial seeding at 50,000 cells/well in 4-well Nunc™ Lab-Tek™ Chamber Slides, NPs were administered at a concentration of 1.0×10^{11} NP/mL. Cells were incubated with particles for a period of two hours

before they were washed three times with PBS and fresh media was added to each well. Cells were then cultured for an additional five days. On each day, one sample from each experimental group was washed, fixed, and stained according to an established protocol. In brief, cells were washed three times with warm PBS and fixed in 3.7% paraformaldehyde solution in PBS for 15 minutes. Finally, cells were washed three times with fresh PBS, dried, and samples were mounted using Prolong™ Diamond with DAPI Antifade Mountant to both stain the nucleus and preserve the samples.

Samples from each experimental group and time point were imaged using CLSM (confocal laser scanning microscopy). Multiple Z-stacks from each sample were taken, maintaining constant laser settings across all samples. GFP signal, normalized to that of the nucleus, was quantified using ImageJ software.

In vitro STAT3 silencing via albumin nanoparticle delivered siRNA

To validate the ability of STAT3 siRNA delivered via SPNPs, particles loaded with siRNA against STAT3 were synthesized as described above. GL26 cells were cultured according to a previously described protocol. Twelve hours after initial seeding at 300,000 cells/well in 6-well cell culture plates, NPs were administered at a concentration of 1.0×10^{11} NP/mL. Cells were incubated with particles for a period of two hours before they were washed three times with PBS and fresh media was added to each well. Cells were then cultured for an additional three days with a daily exchange of fresh media. Whole cell extracts were prepared by lysing the cells with RIPA buffer for 5 minutes on ice, then centrifuged at 10,000g for 5 minutes at 4°C to remove cellular debris. Protein concentration was quantified using the Pierce BCA Protein Assay Kit. STAT3 expression was quantified using the ProteinSimple capillary electrophoresis-based western blot assay and normalized to the expression of β-actin.

Intracranial GBM models

Six to eight-week-old female C57BL/6 were purchased from Jackson Laboratory (Bar Harbor, ME) and were housed in pathogen free conditions at the University of Michigan. All experimental studies were performed in compliance with Institutional Animal Care & Use Committee (IACUC). Orthotopic tumors were established in C57BL/6 mice by stereotactically injecting 20,000 GL26, GL26-Cit or 60,000 GL26-OVA cells into the right striatum of the brain using a 22-gauge Hamilton syringe (1 µL over 1 minute) with the following coordinates: +1.00 mm anterior, 2.5 mm lateral, and 3.00 mm deep.

Intratumoral diffusion of iRGD functionalized albumin nanoparticles

To assess Albumin NP accumulation within the GBM tumor microenvironment, Alexa Flour 647 dye was loaded into Albumin NP, which were administered intratumorally into GBM bearing mice. Fourteen days post GL26-mtomato tumor implantation, mice (n=2/group) were intratumorally injected with 3.6×10^8 or 3.6×10^9 Alexa Flour 647 loaded Albumin NP in 3uL volume. From each group, mice were transcardially perfused 4h or 24h after NP administration, and brains were processed for imaging. Alexa Flour 647 dye loaded Albumin NP accumulation within the TME was imaged with confocal microscopy (Carl Zeiss: MIC System) at 5x and 20x magnification.

Intravenous iRGD Nanoparticle Delivery

To assess the accumulation of systemically administered iRGD-Albumin NPs within the GBM tumor microenvironment, Alexa Flour 647 dye was loaded into the NPs, which were injected i.v. into GBM bearing mice. Seven days post GL26-cit tumor implantation, mice were i.v. injected with 2.0×10^{11} NPs in 100 µL volume. From each group, mice were transcardially perfused at 4h (n=3 mice) and 24hrs (n=3 mice), and brains were processed for imaging. Accumulation of

NPs within the tumor microenvironment was imaged with confocal microscopy (Carl Zeiss: MIC System) at 63x with oil-immersion lens.

Biodistribution of iRGD Nanoparticles Post Systemic Delivery

To evaluate the biodistribution of iRGD-albumin NP *in vivo*, NPs were loaded with Alexa Fluor™ 647 dye. C57BL/6 mice bearing GL26 tumors (n=5) were injected intravenously (i.v) with 2.0x 10^{11} Alexa Fluor™ 647 iRGD-albumin or albumin alone NPs in 100 µL volume 7, 10, and 13 days post tumor implantation. For the control group, tumor naïve mice were injected i.v with 2.0x 10^{11} Alexa Fluor™ 647 iRGD-albumin or albumin alone NPs in 100 µL volume. From each group, mice were transcardially perfused 24hrs post the last injection of NPs, and vital organs (i.e., lungs, spleen, liver, brain, and kidneys) were harvested. Fluorescent signal within each organ was measured with IVIS spectrum analysis.

To assess the iRGD-Albumin NPs' accumulation within the GBM tumor microenvironment, NPs loaded with Alexa Fluor™ 647 dye were administered i.v into GBM bearing mice. Seven days post GL26-cit tumor implantation, 2.0x 10^{11} NPs in 100 µL volume were administered i.v. to mice (n=4). Then, mice were transcardially perfused at either at 4 h (n=2) or 24 h (n=2) post the NP injection. Brains were collected and processed for imaging. Accumulation of NPs within the tumor microenvironment was imaged with confocal microscopy (Carl Zeiss: MIC System) at 63x with oil-immersion lens.

STAT3 and downstream protein expression following systemic administration of STAT3

To validate the ability of STAT3 siRNA loaded SPNPs to reach the tumor in-vivo, particles loaded with siRNA against STAT3 were synthesized as described above. C57BL/6 mice bearing GL26 tumors (n=5) were injected intravenously (i.v) with 2.0x 1011Alexa Fluor SPNPs, STAT3i SPNPs, or free STAT3i in 100 µL volume on 5, 7, 11, 15, 18 and 22 days' post tumor

implantation. For the control group, tumor-bearing mice were injected i.v with an equal volume of saline. Mice from each group were transcardially perfused with Tyrode's solution 24hrs post the last injection of NPs or saline and brains were extracted. Tumors were dissected from the brain, and single cell suspension was obtained. Whole cell lysates were prepared by incubating the dissociated cells pellet with protease inhibitors and 1.4mL RIPA lysis buffer on ice for 5 minutes. Resulting cell lysates were centrifuged at 13000 RPM at 4°C for 10 minutes and supernatants were collected to determine protein concertation in comparison to standard bovine serum albumin (BSA) protein concentrations through bicinchonicinc acid (BCA) assay. STAT3 and downstream target's protein expression was quantified using the ProteinSimple capillary electrophoresis-based western blot assay and normalized to total protein expression.

Therapeutic study in tumor bearing animals

To evaluate the therapeutic efficacy of iRGD-Albumin NPs loaded with STAT3*i*, saline, 2.0 x 10^{11} of free-NPs, STAT3*i*-SPNPs or 330*μ*g of free-STAT3*i* were administered intravenously in 100 µL volume into GL26 tumor bearing mice on 5, 8, 11, 15, 18, 22 and 25 days post tumor implantation. Also, a dose of 2 Gy Irradiation (IR) was administered to tumor bearing mice 5 days a week for two weeks at 7 days post tumor implantation. Each treatment group consisted of at least n=5 mice. When mice displayed signs of neurological deficits, they were transcardiacly perfused with tyrodes solution and 4% paraformaldehyde (PFA).

Immunohistochemistry

Using the vibratome system, PFA-fixed brains were serially sectioned 50 *μ*m thick and placed in PBS with 0.01% sodium azide. Immunohistochemistry for macrophages was performed by permeabilizing the brain sections with TBS-0.5% Triton-X (TBS-Tx) for 10 min, followed by antigen retrieval at 96 °C with 10 mM sodium citrate (pH 6) for 20 min. Then, the sections were

allowed to cool to room temperature (RT) and washed 5 times with TBS-Tx (5 min per wash). Next, the brain sections were blocked with 10% goat serum in TBS-Tx for 1 h at RT followed by overnight primary antibody F4/80 (BioRad, MCA497GA, 1:250) incubation at RT. The primary antibody was diluted in 1% goat serum in TBS-Tx. The next day, brain sections were washed with TBS-Tx 5 times and incubated in fluorescent-dye conjugated secondary antibody (Thermofisher, A21209, 1:1000) diluted in 1% goat serum TBS-Tx in the dark for 6 hrs. Finally, brain sections were washed in PBS 3 times and mounted onto microspore slides and coverslipped with ProLong Gold. High magnification images at 63X were obtained using confocal microscopy (Carl Zeiss: MIC-System).

H&E staining on whole brain sections was performed as described by us previously. Also, H&E staining was performed on livers that were embedded in paraffin and sectioned 5μm thick using the microtome system. Brightfield images of the stains were obtained using Olympus BX53 microscope.

ELISA

To evaluate whether human albumin within the NPs is immunogenic, expression of antibodies against human albumin or mouse albumin in the serum of mice treated with saline, free-NPs, free-STAT3*i*, STAT3*i* SPNPs, IR, or STAT3*i* SPNPs + IR was determined using ELISA. Briefly, 96-wells' plates were coated with NPs loaded with either mouse albumin or human albumin overnight at 4°C. The coated plates were washed the next day with 1X PBS + 0.05% Tween-20 (PBS-Tween) 5 times, and then blocked with PBS-Tween containing 5% goat serum at RT for 2 h. This was followed by 5 more washes with PBS-Tween. Next, mouse serum diluted 1:100 from each treatment groups was added to the NP coated wells in a 100 µL volume and incubated at 4 °C for 24 h. For a positive control, primary anti-body against human serum albumin (abcam, ab10241,

1:1000) or mouse serum albumin (abcam, ab34807, 1:1000) was added to the appropriate wells. The next day, the plates were washed five times with PBS-Tween and 100ul of anti-mouse (Thermofisher, 62-6520, 1:3000) or anti-rabbit (abcam, ab6721, 1:3000) secondary antibody was added to the appropriate plate, followed by 1 h incubation at 37°C. For a negative control, secondary anti-body against human serum albumin or mouse serum albumin was added to the appropriate wells. Plates were then washed 5 times with PBS-Tween. Substrate solution (TMB) was added and the plate was incubated in the dark at RT for 30min and the reaction was quenched by the addition of 2M Sulfuric Acid. Plates were read on a 96-well plate reader (Spectramax Plus, Molecular Devices) at O.D. 450nm.

Flow cytometry

Antibodies for flow cytometry analysis were obtained from Biolegend unless indicated otherwise. To assess the immune cell population within the GL26-OVA tumor microenvironment, two days post STAT3*i* alone, empty SPNP, STAT3*i* SPNP or STAT3*i* SPNP + IR treatment detailed above, mice were euthanized and the tumor mass with the brain was dissected and homogenized using Tenbroeck (Corning) homogenizer in DMEM media containing 10% FBS. Tumor infiltrating immune cells was enriched with 30%-70% Percoll (GE Lifesciences) density gradient and the cells were resuspended in PBS containing 2% FBS (flow buffer). Live/dead staining was carried out using fixable viability dye (eBioscience). Non-specific antibody binding was blocked with CD16/CD32. Dendritic cells were labeled with CD45, CD11c, and B220 antibodies. Plasmacytoid dendritic cells (pDCs) were identified as $CD45^{+}/CD11c^{+}/B220^{+}$ and conventional dendritic (cDCs) cells were identified as $CD45^{+}/CD11c^{+}/B220^{-}$. Macrophages were labeled with CD45, F4/80, and CD206 antibodies. M1 macrophages were identified as $CD45^{+}/$ $F4/80^{+}/$ $CD206^{low}$ and M2 macrophages were identified as $CD45^{+}/$ $F4/80^{+}/$ $CD206^{high}$. Tumor

specific T cells were labeled with CD45, CD3, CD8 and SIINFEKL-H2Kb-tetramer. Granzyme B and IFNγ were stained using BD intracellular staining kit following the manufacturer's instructions. For T cell functional analysis, purified immune cells from the tumor microenvironment were stimulated with 100 µg/mL of GL26-OVA lysate for 16h in DMEM media containing 10% FBS followed by 6 hrs incubation with Brefeldin and monensin. For integrin αvβ3 and αvβ5 analysis, untreated GL26-tumor bearing mice were euthanized 23 dpi and both tumor bearing hemisphere and the contralateral hemisphere were dissected. Cells were dissociated from both the hemispheres into single cell suspension and CD45 cells were labeled with magnetic beads (Miltenyi) using the manufactures' instructions at 4 °C. Purified cells were washed and passed through a preconditioned MS column placed in the magnetic field of a MACS separator. Cells that were negative for CD45 were collected, resuspeneded in flow buffer and labeled with αvβ3 (Novus, NBP2-67557) and αvβ5 (BD Bioscience, 565836) for flowcytometry analysis. All stains were carried out for 30min at 4°C with 3X flow buffer washes between live/dead staining, blocking, surface staining, cell fixation, intracellular staining and data measurement. All flow measurements have been made utilizing with FACSAria flow cytometer (BD Bioscience) and analyzed using Flow Jo version 10 (Treestar).

1. Alifieris, C. & Trafalis, D. T. Glioblastoma multiforme: Pathogenesis and treatment. *Pharmacol. Ther.* **152**, 63–82 (2015).

2. Davis, M. E. Glioblastoma: Overview of Disease and Treatment. *Clin J Oncol Nurs* **20**, 1–14 (2016).

3. Stupp, R. *et al.* Radiotherapy plus concomitant and adjuvant temozolomide for glioblastoma. *N. Engl. J. Med.* **352**, 987–96 (2005).

4. Van Tellingen, O. *et al.* Overcoming the blood-brain tumor barrier for effective glioblastoma treatment. *Drug Resist. Updat.* **19**, 1–12 (2015).

5. CBTRUS. CBTRUS Statistical Report: Primary Brain and Central Nervous System Tumors Diagnosed in the United States in 2004-2008. (2012).

6. Assi, H. H. *et al.* Preclinical characterization of signal transducer and activator of transcription 3 small molecule inhibitors for primary and metastatic brain cancer therapy. *J. Pharmacol. Exp. Ther.* **349**, 458–69 (2014).

7. Abou-Ghazal, M. *et al.* The incidence, correlation with tumor-infiltrating inflammation, and prognosis of phosphorylated STAT3 expression in human gliomas. *Clin Cancer Res* **14**, 8228–8235 (2008).

8. Kim, J. E., Patel, M., Ruzevick, J., Jackson, C. M. & Lim, M. STAT3 activation in glioblastoma: Biochemical and therapeutic implications. *Cancers (Basel).* **6**, 376–395 (2014).

9. Ganguly, D. *et al.* The critical role that STAT3 plays in glioma-initiating cells: STAT3

addiction in glioma. *Oncotarget* **9**, 22095–22112 (2018).

10. de la Iglesia, N., Puram, S. V & Bonni, A. STAT3 regulation of glioblastoma pathogenesis. *Curr. Mol. Med.* **9**, 580–90 (2009).

11. Gajbhiye, V. & Jain, N. K. The treatment of Glioblastoma Xenografts by surfactant conjugated dendritic nanoconjugates. *Biomaterials* **32**, 6213–6225 (2011).

12. Gao, H. *et al.* Whole-cell SELEX aptamer-functionalised poly(ethyleneglycol)-poly(ε-caprolactone) nanoparticles for enhanced targeted glioblastoma therapy. *Biomaterials* **33**, 6264–6272 (2012).

13. Shi, K. *et al.* Arginine-glycine-aspartic acid-modified lipid-polymer hybrid nanoparticles for docetaxel delivery in glioblastoma multiforme. *J. Biomed. Nanotechnol.* **11**, 382–391 (2015).

14. Ganipineni, L. P. *et al.* Paclitaxel-loaded multifunctional nanoparticles for the targeted treatment of glioblastoma. *J. Drug Target.* **27**, 614–623 (2019).

15. Kang, T. *et al.* Enhancing Glioblastoma-Specific Penetration by Functionalization of Nanoparticles with an Iron-Mimic Peptide Targeting Transferrin/Transferrin Receptor Complex. *Mol. Pharm.* **12**, 2947–2961 (2015).

16. Kang, T. *et al.* Synergistic targeting tenascin C and neuropilin-1 for specific penetration of nanoparticles for anti-glioblastoma treatment. *Biomaterials* **101**, 60–75 (2016).

17. Yang, F. Y. *et al.* Focused ultrasound and interleukin-4 receptor-targeted liposomal doxorubicin for enhanced targeted drug delivery and antitumor effect in glioblastoma multiforme. *J. Control. Release* **160**, 652–658 (2012).

18. Zhou, J. *et al.* Highly penetrative, drug-loaded nanocarriers improve treatment of glioblastoma. *Proc. Natl. Acad. Sci. U. S. A.* **110**, 11751–6 (2013).

19. Householder, K. T. *et al.* Intravenous delivery of camptothecin-loaded PLGA nanoparticles for the treatment of intracranial glioma. *Int. J. Pharm.* **479**, 374–380 (2015).

20. Gaudin, A. *et al.* PEGylated squalenoyl-gemcitabine nanoparticles for the treatment of glioblastoma. *Biomaterials* **105**, 136–144 (2016).

21. King, A. R. *et al.* Local DNA Repair Inhibition for Sustained Radiosensitization of High-Grade Gliomas. *Mol. Cancer Ther.* **16**, 1456–1469 (2017).

22. Zhang, C.-X. *et al.* A nanostructure of functional targeting epirubicin liposomes dually modified with aminophenyl glucose and cyclic pentapeptide used for brain glioblastoma treatment. *Oncotarget* **6**, (2015).

23. Kaluzova, M., Bouras, A., Machaidze, R. & Hadjipanayis, C. G. Targeted therapy of glioblastoma stem-like cells and tumor non-stem cells using cetuximab-conjugated iron-oxide nanoparticles. *Oncotarget* **6**, (2015).

24. Bouras, A., Kaluzova, M. & Hadjipanayis, C. G. Radiosensitivity enhancement of radioresistant glioblastoma by epidermal growth factor receptor antibody-conjugated iron-oxide nanoparticles. *J. Neurooncol.* **124**, 13–22 (2015).

25. Cohen, Z. R. *et al.* Localized RNAi therapeutics of chemoresistant grade IV glioma using hyaluronan-grafted lipid-based nanoparticles. *ACS Nano* **9**, 1581–1591 (2015).

26. Danhier, F., Messaoudi, K., Lemaire, L., Benoit, J. P. & Lagarce, F. Combined anti-Galectin-1 and anti-EGFR siRNA-loaded chitosan-lipid nanocapsules decrease temozolomide resistance in glioblastoma: In vivo evaluation. *Int. J. Pharm.* **481**, 154–161

(2015).

27. Erel-Akbaba, G. *et al.* Radiation-induced targeted nanoparticle-based gene delivery for brain tumor therapy. *ACS Nano* **13**, 4028–4040 (2019).

28. Seo, Y. E. *et al.* Nanoparticle-mediated intratumoral inhibition of miR-21 for improved survival in glioblastoma. *Biomaterials* **201**, 87–98 (2019).

29. Agemy, L. Targeted nanoparticle enhanced proapoptotic peptide as potential therapy for glioblastoma. *Proc. …* **108**, 17450–17455 (2011).

30. Gu, G. *et al.* The influence of the penetrating peptide iRGD on the effect of paclitaxel-loaded MT1-AF7p-conjugated nanoparticles on glioma cells. *Biomaterials* **34**, 5138–5148 (2013).

31. Tabatabai, G. *et al.* Targeting integrins in malignant glioma. *Target. Oncol.* **5**, 175–181 (2010).

32. Bello, L. *et al.* Alpha(v)beta3 and alpha(v)beta5 integrin expression in glioma periphery. *Neurosurgery* **49**, 380–389; discussion 390 (2001).

33. Desai, N., Trieu, V., Damascelli, B. & Soon-Shiong, P. SPARC Expression Correlates with Tumor Response to Albumin-Bound Paclitaxel in Head and Neck Cancer Patients. *Transl. Oncol.* **2**, 59–64 (2009).

34. Iancu, C. *et al.* Enhanced laser thermal ablation for the in vitro treatment of liver cancer by specific delivery of multiwalled carbon nanotubes functionalized with human serum albumin. *Int. J. Nanomedicine* **6**, 129–141 (2011).

35. Kunigal, S. *et al.* SPARC-Induced Migration of Glioblastoma Cell Lines via uPA- uPAR

Signaling and Activation of Small GTPase RhoA Sateesh. *PLoS One* **32**, 736–740 (2017).

36. Golembieski, W. A. & Rempel, S. A. cDNA array analysis of SPARC-modulated changes in glioma gene expression. *J. Neurooncol.* **60**, 213–226 (2002).

37. Schnitzer, J. E. Gp60 Is an Albumin-Binding Glycoprotein Expressed By Continuous Endothelium Involved in Albumin Transcytosis By Continuous Endothelium Glycoprotein Expressed Involved in Albumin Transcytosis. *Am J Physiol.* **262**, 246–54 (1992).

38. Hwang, S. *et al.* Anisotropic hybrid particles based on electrohydrodynamic co-jetting of nanoparticle suspensions. *Phys. Chem. Chem. Phys.* **12**, 11894 (2010).

39. Roh, K., Martin, D. C. & Lahann, J. Biphasic Janus particles with nanoscale anisotropy. *Nat. Mater.* **4**, 759–763 (2005).

40. Rahmani, S. *et al.* Engineering of nanoparticle size via electrohydrodynamic jetting. *Bioeng. Transl. Med.* **1**, 82–93 (2016).

41. Sugahara, K. N., Teesalu, T., Karmali, P. P. & Ramana, V. Co-administration of a Tumor-Penetrating Peptide Enhances the Efficacy of Cancer Drugs. **328**, 1031–1035 (2010).

42. Sugahara, K. N. *et al.* Tissue-Penetrating Delivery of Compounds and Nanoparticles into Tumors. *Cancer Cell* **16**, 510–520 (2009).

43. Liu, X. *et al.* Tumor-penetrating peptide enhances transcytosis of silicasome-based chemotherapy for pancreatic cancer. *J. Clin. Invest.* **127**, 2007–2018 (2017).

44. Hu, C. *et al.* Coadministration of iRGD with Multistage Responsive Nanoparticles Enhanced Tumor Targeting and Penetration Abilities for Breast Cancer Therapy. *ACS*

Appl. Mater. Interfaces **10**, 38659–38662 (2018).

45. Zhang, J. *et al.* Co-delivery of paclitaxel and tetrandrine via iRGD peptide conjugated lipid-polymer hybrid nanoparticles overcome multidrug resistance in cancer cells. *Sci. Rep.* **7**, 1–14 (2017).

46. Ma, L. *et al.* IRGD-functionalized PEGylated nanoparticles for enhanced colon tumor accumulation and targeted drug delivery. *Nanomedicine* **12**, 1991–2006 (2017).

47. Behr, J. P. The proton sponge. A trick to enter cells the viruses did not exploit. *Chimia (Aarau).* **51**, 34–36 (1997).

48. Pratt, A. J. & MacRae, I. J. The RNA-induced silencing complex: A versatile gene-silencing machine. *J. Biol. Chem.* **284**, 17897–17901 (2009).

49. Dominska, M. & Dykxhoorn, D. M. Breaking down the barriers: siRNA delivery and endosome escape. *J. Cell Sci.* **123**, 1183–1189 (2010).

50. Barua, S. & Mitragotri, S. Challenges associated with penetration of nanoparticles across cell and tissue barriers: A review of current status and future prospects. *Nano Today* **9**, 223–243 (2014).

51. Shi, J., Kantoff, P. W., Wooster, R. & Farokhzad1, O. C. Cancer nanomedicine: Challenges and opportunities. *Med. J. Aust.* **203**, 204-205.e1 (2015).

52. Candolfi, M. *et al.* Intracranial glioblastoma models in preclinical neuro-oncology: Neuropathological characterization and tumor progression. *J. Neurooncol.* **85**, 133–148 (2007).

53. Longmier, M., Choyke, P. L. & Kobayashi, H. Clearance Properties of Nano-sized

Particles and Molecules as Imaging Agents: Consideration and Caveats. *Nanomedicine (Lond)* **3**, 703–717 (2012).

54. Zheng, M., Tao, W., Zou, Y., Farokhzad, O. C. & Shi, B. Nanotechnology-Based Strategies for siRNA Brain Delivery for Disease Therapy. *Trends Biotechnol.* **36**, 562–575 (2018).

55. You, S. *et al.* Disruption of STAT3 by Niclosamide Reverses Radioresistance of Human Lung Cancer. *Mol. Cancer Ther.* **13**, 606–616 (2014).

56. Li, X., Wang, H., Lu, X. & Di, B. Silencing STAT3 with short hairpin RNA enhances radiosensitivity of human laryngeal squamous cell carcinoma xenografts in vivo. *Exp. Ther. Med.* **1**, 947–953 (2010).

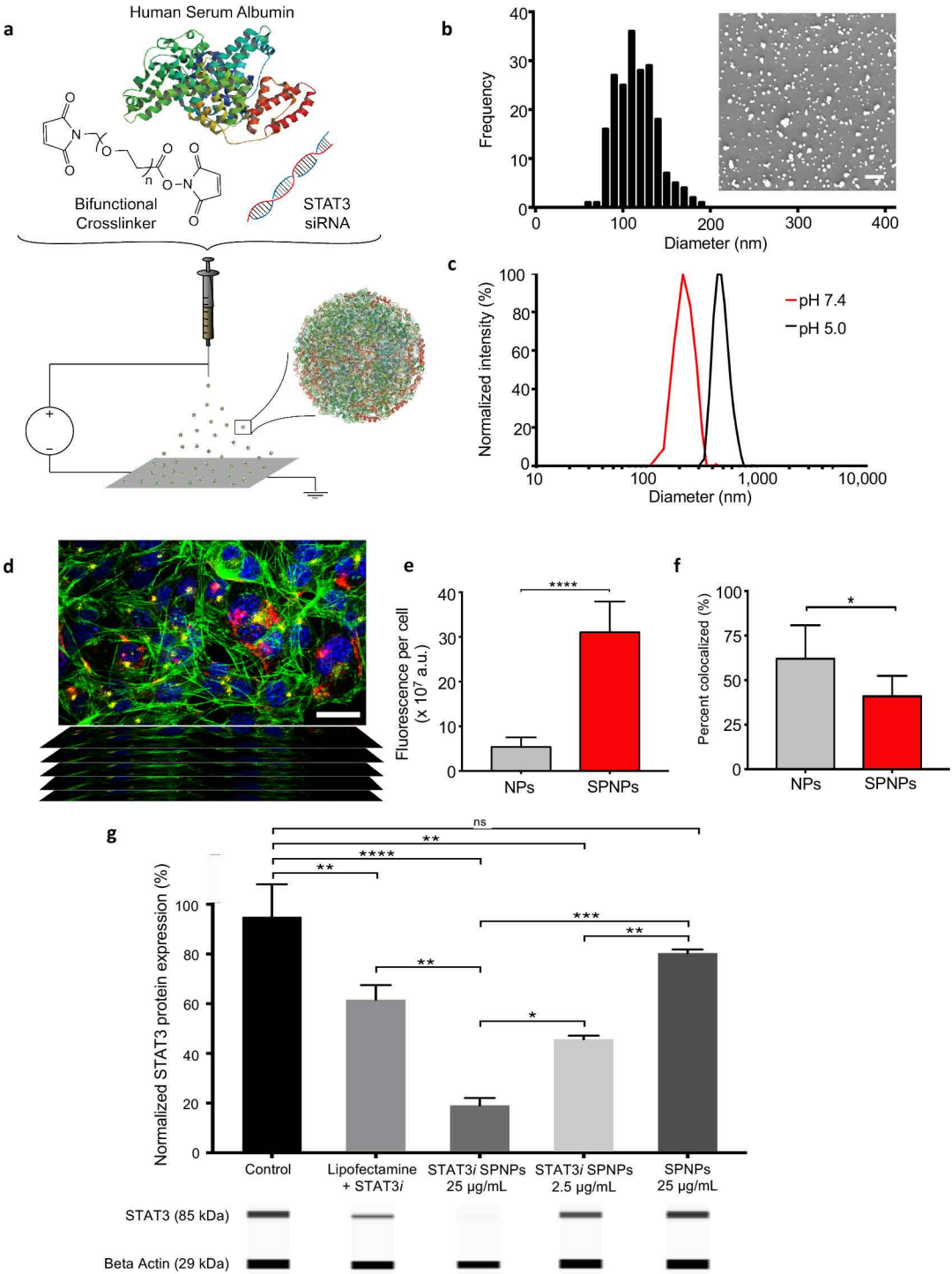

Fig. 1: STAT3 expression is effectively silenced in vitro by siRNA-loaded SPNPs. a, Schematic of jetting formulation for crosslinked, STAT3i-loaded, iRGD-conjugated, targeted albumin nanoparticles (STAT3i SPNPs) **b,** Particle size characterization and analysis was performed using Scanning Electron Microscopy (SEM). Average particle diameter, 115 ± 23.4 nm. Scale bar 1 μm. **c**, Particles undergo swelling in their hydrated state and further swell at reduced pH. Average diameters: pH 7.4, 220 ± 26.1 nm. pH 5.0, 295 ± 31.2 nm. **d,** Representative confocal z-stack image of cells seeded in the presence of SPNPs **e,** Local release of iRGD from SPNPs increases particle uptake in GL26 glioma cells by greater than five-fold. **f,** Internalized SPNPs colocalize with lysosomes to a lesser extent than untargeted particles. **g,** STAT3 siRNA-loaded SPNPs significantly reduce *in vitro* expression of target protein in GL26 glioma cells compared to untreated and empty particle control groups. Bars represent mean ± standard error, (****p<0.0001, ***p<0.0005, **p<0.005, *p<0.05, two-way ANOVA test) (n ≥ 3 wells/treatment group).

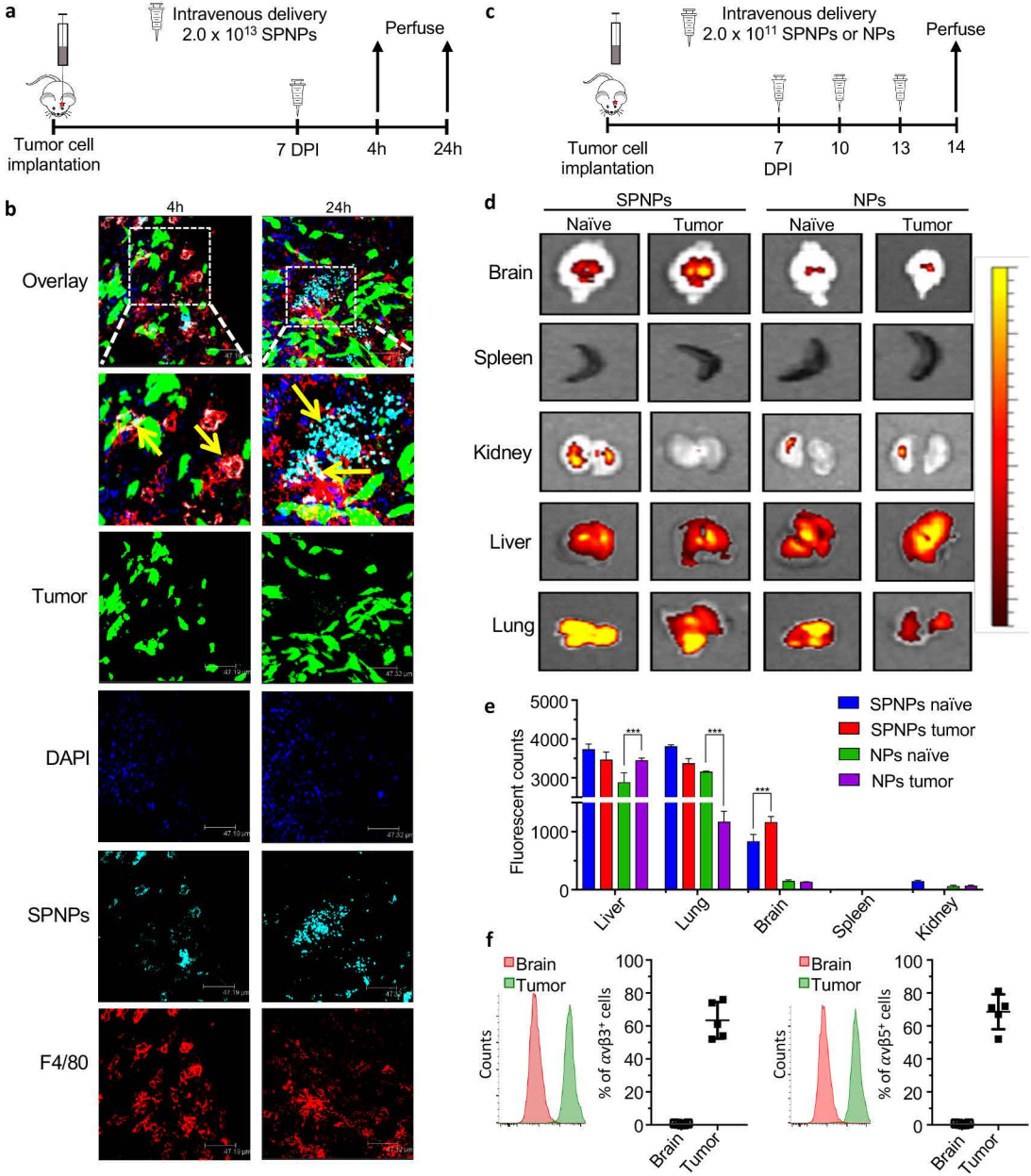

Fig. 2: In vivo brain targeting and biodistribution of SPNPs. a, Timeline for the tumor targeting study. Mice were IV administrated a single 2.0 x 10^{13} SPNPs or Empty-NPs dose via the tail vein seven days post GL26 tumor cells implantation. Confocal imaging of sectioned brains was performed 4 and 24 hours post particle administration. **b,** Alexa Fluor 647 labeled SPNPs (cyan) colocalize (indicated with yellow arrows) with macrophages (red) and tumor cells (green, mCitrine). Less NPs are observed in the tumor microenvironment 4h post systemic delivery compared to 24h. **c**, Timeline representation of the biodistribution study. Mice were IV administered 2.0 x 10^{11} SPNPs or Empty-NPs 7, 10, and 13 days post tumor cell implantation or saline injection. **d,** Fluorescence imaging of tumor-naive and tumor-bearing mice organs sacrificed at 24h post final NP delivery. **e**, Quantitative analysis of NP biodistribution within the tumor and peripheral organs (****$p < 0.00001$, **$p < 0.001$, *$p < 0.05$, two-way ANOVA test) **f,** Quantitative flow cytometry results of avβ3 and avβ5 integrin expression in normal brain tissue and GL26 tumors.

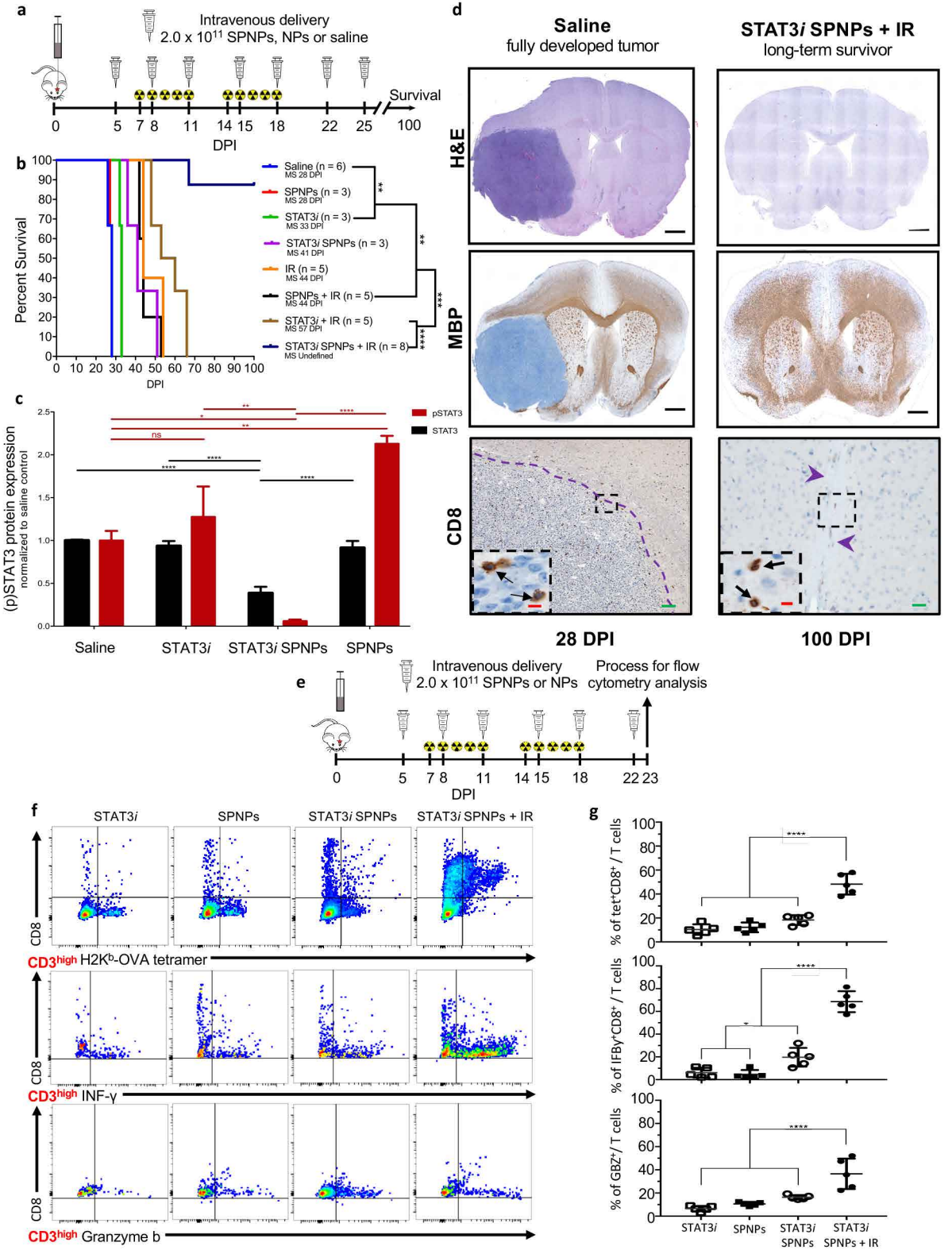

Fig. 3: Systemic delivery of STAT3i SPNPs in combination with radiotherapy (IR) results in increased survival and primes an adaptive immune response. **a**, Timeline of treatment for the combined NP + IR survival study. **b**, Kaplan-Meier survival curve. Significant increase in median survival is observed in all groups receiving IR. Mice (7/8) treated with STAT3*i* SPNPs + IR reach long-term survival timepoint (100 DPI) with no signs of residual tumor. **c**, Quantified STAT3 expression for resected brains from the survival study, brains were collected when mice displayed signs of neurological deficits. A significant reduction is STAT3 and pSTAT3 expression was observed in the STAT3*i* SPNP cohort relative to untreated control. Both soluble STAT3*i* and empty SPNPs (with no siRNA) did not have high total STAT3 expression but they had increased levels of active phosphorylated STAT3 expression (pSTAT3). Bars represent the mean relative to untreated control ± standard error ($n \geq 3$). ****$p < 0.0001$, **$p < 0.005$, *$p < 0.05$, ; unpaired t-test. **d**, IHC staining for untreated control and STAT3*i* SPNP + IR long-term survivor. (Top) H&E staining shows the fully formed tumor in the saline control group (28 DPI). When treated with the combination of STAT3*i* SPNPs + IR, no tumor or signs of necrosis were observed. (Middle) MBP staining shows preserved brain structures with no apparent changes in oligodendrocyte integrity in mice that received STAT3*i* SPNPs + IR treatment compared to the saline control. (Bottom) CD8 staining shows no overt inflammation in mice that received STAT3*i* SPNPs + IR treatment compared to the saline control. **e**, Timeline of TME immune population by flow cytometry. **f**, Flow cytometry analysis of CD8 cells in the TME. Representative flow plots for each group are displayed. **g**, Quantitative analysis of tumor-specific $CD8^+$ T cells within the TME. GL26-OVA tumors were analyzed by staining for the SIINFEKL-K^b tetramer. Activation status of $CD8^+$ T cells within the TME was analyzed by staining for granzyme B (Gzb) and IFNγ after stimulation with the tumor lysate.. ****$p < 0.0001$; unpaired t-test. Bars represent mean ± SEM ($n = 5$ biological replicates).

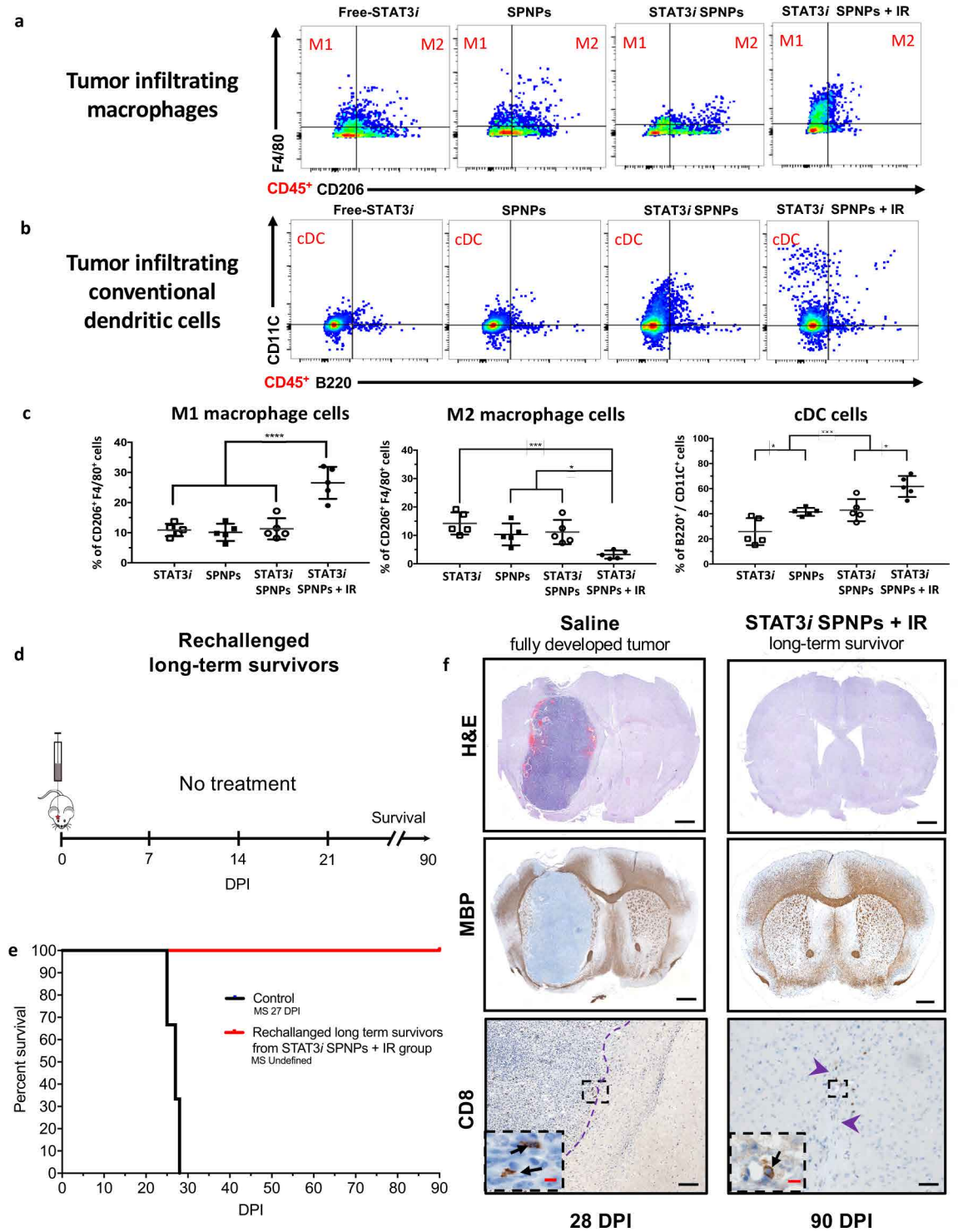

Fig. 4: SPNPs protect against GBM rechallenge. **a-b**, Flow analysis of tumor infiltrating **a**, macrophage and **b**, conventional dendritic cell (cDCs) populations in the tumor microenvironment (TME) following NP + IR treatment regimen. **c**, Quantitative analysis of the immune cellular infiltrates showed a shift in the relative macrophage (M1 *vs.* M2) present in the TME. In the free siRNA, empty SPNPs, and STAT3*i* SPNPs groups no significant change in the macrophage population were observed. Conversely, STAT3*i* SPNPs + IR treatment induces both a surge of approximately 2.5-fold increase in M1 population and a sharp 3- to 4-fold decrease in M2 macrophages. Among cDCs, progressively larger numbers of the cell population were observed moving from free siRNA to SPNPs groups. The combined treatment of STAT3*i* SPNPs with IR displayed the highest number of cDCs in the brain TME. **d**, Timeline for rechallenging the long-term survivor for STAT3*i* SPNPs + IR survival study rechallenged, where following tumor implantation, no further treatment was provided. **e**, Kaplan-Meier survival curve shows all rechallenged survivors reach a second long-term survival timepoint of 90 DPI in the absence of any therapeutic interventions. **f,** IHC staining (H&E, MBP, and CD8) comparing the brains of untreated and rechallenged long-term survivors. No overt signs of remaining tumor, necrosis, inflammation, or disruption of normal brain architecture was observed in rechallenged long-term survivors from STAT3*i* SPNPs treatment group. Representative flow plots for each group are displayed. ****$p < 0.0001$; unpaired t-test. Bars represent mean ± SEM (n = 5 biological replicates).